

Electronic Supplementary Information

Highly-Emissive Solution-Grown Furan/Phenylene Co-Oligomer Single Crystals

*Maxim S. Kazantsev**, *Ekaterina S. Frantseva*, *Ludmila G. Kudryashova*, *Vladislav G. Konstantinov*,
Artur A. Mannanov, *Tatyana V. Rybalova*, *Elena V. Karpova*, *Inna K. Shundrina*, *Gennadiy N.*
Kamaev, *Maxim S. Pshenichnikov*, *Evgeny A. Mostovich* and *Dmitry Yu. Paraschuk**

CONTENT:	page
1. Experimental details.....	2
2. Synthesis	6
3. Spectra of synthesized compounds	9
4. Thermal and CVA analysis	15
5. Microscopy.....	16
6. X-ray study.....	16
7. Quantum chemistry calculations.....	18
8. OFET Data	20
9. Photoluminescence quantum yield	21
10. Photoluminescence kinetics.....	24
11. References	27

1. Experimental details

Characterization. Combustion analysis was performed with a CHN-analyzer (EURO EA). The NMR spectra ^1H and ^{13}C were recorded with a Bruker AV 400 (400.13 MHz) spectrometer in CDCl_3 . Mass spectra were obtained with a Thermo Electron Corporation DFS mass spectrometer (70 eV) using direct injection, the temperature of the ionization chamber was 220–270 °C. IR spectra were recorded in the transmission mode with a Bruker Tensor 27 FT-IR spectrometer in potassium bromide pellets. Thermogravimetric analysis and differential scanning calorimetry measurements were performed using a NETZSCH STA 409 instrument at a heating rate of 10 °C/min in an inert (He) or oxidizing ($\text{He}:\text{O}_2 = 80:20$) atmosphere. Cyclic voltammetry measurements were performed in CH_2Cl_2 solution with a computer controlled P-8nano potentiostat/galvanostat (Elins, Russia) in combination with three-electrode cell (Gamry), 0.1 M tetrabutylammonium hexafluorophosphate being used as supporting electrolyte. The Pt, Pt wire and Ag/AgCl were used as working, counter and reference electrodes, respectively. The reference electrode was calibrated by measuring the redox potential of ferrocene. UV/VIS spectra were recorded in a CH_3CN diluted solution using a quartz cuvette and in the film drop-casted on CaF_2 substrate with a Varian Cary 5000 UV-VIS-NIR spectrophotometer. Fluorescence spectra in solution were recorded with Varian Cary Eclipse fluorescence spectrophotometer.

Crystal growth and analysis. For crystal growth solvent-antisolvent crystallization was used.^{1,2} Powder of BPFB was dissolved in toluene (c.a. 0.8 mg/ml) at room temperature. The solution was filtered through the PTFE filter (0.2 μm) and the vial with the solution was placed into the closed vessel containing isopropanol. After growth period (typically overnight ~ 14 hours) the crystals were extracted and dried in ambient conditions. The crystals were examined using optical microscope (MP-7, «Lomo», Russia) in transmitted light through crossed polarizers and under blue laser irradiation (405 nm). The single crystals for further studies were carefully selected to have no cracks, outgrowths and other visible defects. The thickness of the crystals was measured using an interferometer MII-4

(«Lomo», Russia). The surface of the crystals was studied by atomic-force microscopy (Integra-Spectra, NT-MDT) in the tapping mode.

The X-ray diffraction experiments were performed using a Bruker KAPPA APEX II diffractometer with graphite monochromated MoK α radiation. Integration and scaling of the intensity data were accomplished using SAINT.³ Absorption corrections were applied using SADABS.⁴ The structure was solved by direct methods using the SHELXS-97.⁵ Refinement was carried out using the full-matrix least-squares technique using SHELXL.⁵ All non-hydrogen atoms were refined anisotropically. Hydrogen atom positions were calculated geometrically and refined isotropically using the riding model. [CCDC contains the supplementary crystallographic data for this paper as supplementary publication no. CCDC-1478328. These data can be obtained free of charge from The Cambridge Crystallographic Data Centre via www.ccdc.cam.ac.uk/data_request/cif.]

Single-crystal field-effect transistors. Single crystal organic field-effect transistors were fabricated on glass substrates using top-contact top-gate configuration reported elsewhere.⁶ The crystals were attached to the substrates using cyanoacrylate glue. Colloidal graphite suspension (PELCO, TED PELLA, INC) was used to paint the source and drain contacts on the top of single crystals. The OFET channel width and length were measured using an optical microscope. As a top dielectric layer parylene N was deposited from [2,2]paracyclophane (Sigma Aldrich), as described elsewhere.⁷ Its thickness (typically 1.3–1.7 μm) was measured using an interferometer MII-4 («Lomo», Russia). The dielectric capacitance (1.4–1.8 nF/cm²) was calculated according to the thickness and the dielectric constant of parylene N. The gate electrode was painted on the surface of the dielectric layer using graphite paste. OFET current-voltage characteristics were recorded using a source-meter instrument (Agilent B2902A) at dark conditions, ambient atmosphere and room temperature. The voltage sweep rate was 0.3 Vs⁻¹. Both linear and saturation regimes were used for determination of field-effect mobility of OFET samples. The source-drain current (I_{sd}) in the linear and saturation regimes was fitted according to Equations (S1) and (S2), correspondingly:

$$I_{sd} = \frac{W}{L} \mu_{lin} C (V_g - V_{th}) V_{sd} \quad (S1)$$

$$I_{sd}^{1/2} = \left(\frac{W}{2L} \mu_{sat} C \right)^{1/2} (V_g - V_{th}) \quad (S2)$$

Here C is the capacitance per unit area of the insulating layer; W and L are the channel width and length; μ_{sat} and μ_{lin} are the carrier mobilities in saturation and linear regimes; V_g , V_{th} and V_{sd} are the gate, threshold, and source-drain voltages, respectively.

Samples for optical studies. For spectroscopy on liquid BPFB solution, BPFB molecules were dissolved in acetonitrile (CH_3CN) at a concentration of 1 mg/L. The solution was stirred on a magnetic stirrer for ~5 hours at 50°C, cooled down to the room temperature, and placed in a 1-mm-thick quartz cuvette. A BPFB drop-cast sample was prepared by drop-casting BPFB solution in CHCl_3 (0.5 mg/L) on a glass substrate with subsequent drying for at least 30 minutes. To prepare solid solution samples, poly(methyl methacrylate) (PMMA) was dissolved in acetonitrile (CH_3CN) at a concentration of 15 g/L. The solution was stirred on a magnetic stirrer for ~5 hours at 50°C. Then the solution was mixed with 0.01 g/L BPFB/ CH_3CN solution at 1:1 volume ratio. The resulted BPFB concentration in PMMA matrix amounted to 85 mg/L, i.e. one BPFB molecule per 5000 PMMA monomers. The solid solution was prepared by drop-casting from the PMMA-BBFB solution on a glass substrate with subsequent drying for ~2 hours.

Photoluminescence Quantum Yield (PL QY). The PL QY in CH_3CN solution was measured according to the standard procedure, a diluted solution of 1,4-bis-(5-phenyloxazole-2-yl)benzene in ethanol (PL QY = 0.885) was used as a reference standard.⁸ The PL QY in solid samples was measured using a 3.3-inch-diameter integrating sphere (Newport 819C-SL-3.3). The optical output of the integrating sphere was coupled to a spectrometer (InVia, Renishaw). To calibrate the spectral sensitivity of the spectrometer, the sphere was illuminated by an incandescent lamp SI 8-200 (calibrated at the All-Russian Research Institute for Optical and Physical Measurements, Certificate RU 01 № 643/15). Solid samples on glass substrates were excited at 405 nm using a semiconductor

laser. The optical response of the glass substrates was separately checked for not contributing to the measurement. Typical spectra of a BPFb sample recorded in the integrating sphere are shown in **Figure S21a**.

Photoluminescence kinetics. Time-resolved PL kinetics were measured in a streak camera (C5680, Hamamatsu) combined with a polychromator. The samples were excited at the wavelength of 385 nm (liquid and solid solutions) and 400 nm (the single crystal and the drop-cast sample) by 100 fs pulses produced by the doubled output of a Ti:sapphire laser (Coherent Mira). The laser repetition rate was reduced to 1.9 MHz by an external pulse picker (Coherent). The time-resolved PL collected in the 90°-geometry with respect to the excitation beam. For low temperature measurements, the samples were placed in a liquid nitrogen cryostat (Oxford). In all cases, the apparatus response function was ~50 ps.

2. Synthesis

All reagents and solvents were purchased from commercial sources (Sigma-Aldrich, Acros) and were used without additional purification. Reaction mixtures were monitored by TLC using Sorbfil HPTLC-AF-V-UV plates and hexane as eluent. For column chromatography Masherey-Nagel Kieselgel 60 and pure hexane as eluent were used.

Target compound BPFB (**4**) was synthesized by A. Pelter in late 80th through series of Negishi cross-coupling reactions. However, only a few experimental details were described.⁹ In our work, we used another synthetic pathway to BPFB through combination of Stille and Suzuki cross-coupling reactions (Figure S1).

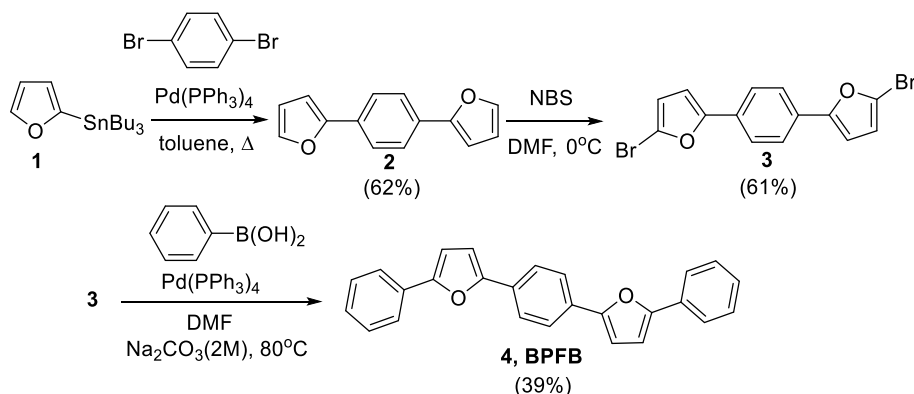


Figure S1. Synthesis of 1,4-bis(5-phenylfuran-2-yl)benzene (**4**, BPFB).

At the first step, Stille coupling of two equivalents of 2-(tributylstannyl)furan **1** and 1,4-dibromobenzene led to precipitation of **2** from the toluene reaction mixture.¹⁰ Then, careful bromination of **2** by NBS under cooling gave selectively 1,4-bis(5-bromofuran-2-yl)benzene (**3**).¹¹ Finally, Suzuki cross-coupling reaction of **3** and 2.2 equivalents of phenylboronic acid gave the target compound BPFB (**4**). High purity BPFB was obtained by multistep vacuum gradient sublimation. It should be noted that furans are oxygen and acid sensitive and one should avoid column chromatography and store furan-containing samples under Ar atmosphere at low temperature.

Synthesis of 2-tri(butyl)stannylfuran **1**.

A solution of furan (5.0 g, 74 mmol) in dry Et₂O (50 ml) was cooled to -78°C. *n*-BuLi (29.4 ml of 2.5 M solution, 74 mmol) was added with a syringe during 30 min. A light yellow solution was formed. The reaction was stirred at -78°C and after 1 h SnBu₃Cl (24.0 g, 74 mmol) was added dropwise. The obtained light yellow solution was kept overnight at r.t. and then was quenched with saturated solution of NaHCO₃ (50 ml). The organic phase was separated. The water phase was extracted with diethyl ether (2×25 ml). The combined diethyl ether phases were washed with water (2×25 ml), dried over MgSO₄ and filtered through short SiO₂ plug (4 cm). Rotary evaporation gave light yellow oil (25.0 g, 98%). The obtained 2-tri(butyl)stannylfuran was used without additional purification.

Synthesis of 1,4-bis(furanyl-2)benzene **2**.

A mixture of 1,4-dibromobenzene (2.87 g, 11.7 mmol), 2-tri(butyl)stannylfuran (**1**) (10.0 g, 28 mmol), and Pd(PPh₃)₄ (675 mg, 0.585 mmol) in dry toluene (20 ml) was refluxed for 24 h under Ar atmosphere. White crystals were formed. The reaction mixture was diluted with excess of hexane and the precipitate was filtered off, washed with hexane (2×10 ml), ethanol (2×10 ml) and dried at air. Flash chromatography on a silica column (using hexane as eluent) followed by rotary evaporation gave white crystals of **2** (1.53 g, 62% yield). ¹H NMR (400 MHz, CDCl₃, δ): 7.71 (s, 4H, ArH), 7.50 (dd, *J*=0.8 Hz, *J*=1.8 Hz, 2H, FuH), 6.69 (dd, *J*=0.8 Hz, *J*=3.4 Hz, 2H, FuH), 6.50 (dd, *J*=1.8 Hz, *J*=3.4 Hz, 2H, FuH); ¹³C NMR (100 MHz, CDCl₃, δ): 153.8, 142.3, 129.8, 124.2, 111.9, 105.3; IR (KBr) 3118, 1513, 1006, 846, 802, 734 cm⁻¹; HRMS(ESI) *m/z*: [M + H]⁺ calcd for C₁₄H₁₀O₂, 210.0675; found, 210.0680.

Synthesis of 1,4-bis(5-bromofuran-2-yl)benzene **3**.

Solution of **2** (1.92 g, 9.13 mmol) in dry DMF (100 ml) was cooled to 0°C. The temperature in the range 0–5°C was maintained and NBS (3.9 g, 21.9 mmol) was carefully added by small portions. Then the reaction was stirred for 2 h at 0°C. After that it was poured into cold water (800 ml). The

precipitate was filtered, washed with water (2×100 ml) and methanol (2×30 ml). Flash chromatography with a silica column using CH₂Cl₂ (with a few drops of NEt₃) followed by rotary evaporation gave white crystals of **3** (3.36 g, 61% yield). ¹H NMR (400 MHz, CDCl₃, δ): 7.63 (s, 4H, ArH), 6.63 (d, *J*=3.4 Hz, 2H, FuH), 6.40 (d, *J*=3.4 Hz, 2H, FuH). HRMS (ESI) *m/z*: [M+H]⁺ calcd for C₁₄H₈⁷⁹Br₂O₂, 365.8886; found, 365.8878.

Synthesis of 1,4-bis(5-phenylfuran-2-yl)benzene **4**, (BPFB).

A mixture of 1,4-bis(5-bromofuran-2-yl)benzene **3** (368 mg, 1 mmol), phenylboronic acid (299 mg, 2.2 mmol), Pd(PPh₃)₄ (116 mg, 0.1 mmol), and Na₂CO₃ (2 M, 10 ml) in DMF (25 ml) was refluxed at 80°C for 24 h under Ar. The precipitate formed was filtered, washed with water (3×10 ml), ethanol (3×10 ml) and hexane (3×10 ml). Gradient sublimation at 230–270°C and 2·10⁻² torr gave yellow crystals of **4** (115 mg, 39%). mp 238°C; ¹H NMR (400 MHz, CDCl₃, δ): 7.78 (s, 4H, -C₆H₄-); 7.76 (m, 4H, PhH); 7.42 (m, 4H, PhH); 7.29 (m, 2H, PhH); 6.78 (dd, *J*=3.4 Hz, 4H, FuH); ¹³C NMR (100 MHz, CDCl₃, δ): 153.6, 153.3, 130.8, 129.7, 128.9, 127.6, 124.1, 123.9, 107.7, 107.6; IR (KBr) 3128, 1608, 1475, 1022, 792, 758 cm⁻¹; UV-vis (CH₃CN): λ_{max} = 373 nm; HRMS (ESI) *m/z*: calcd for C₂₆H₁₈O₂, 362.1301; found, 362.1298. Anal. calcd for C₂₆H₁₈O₂: C, 86.16; H, 5.01; found: C, 85.79; H, 5.07.

3. Spectra of synthesized compounds

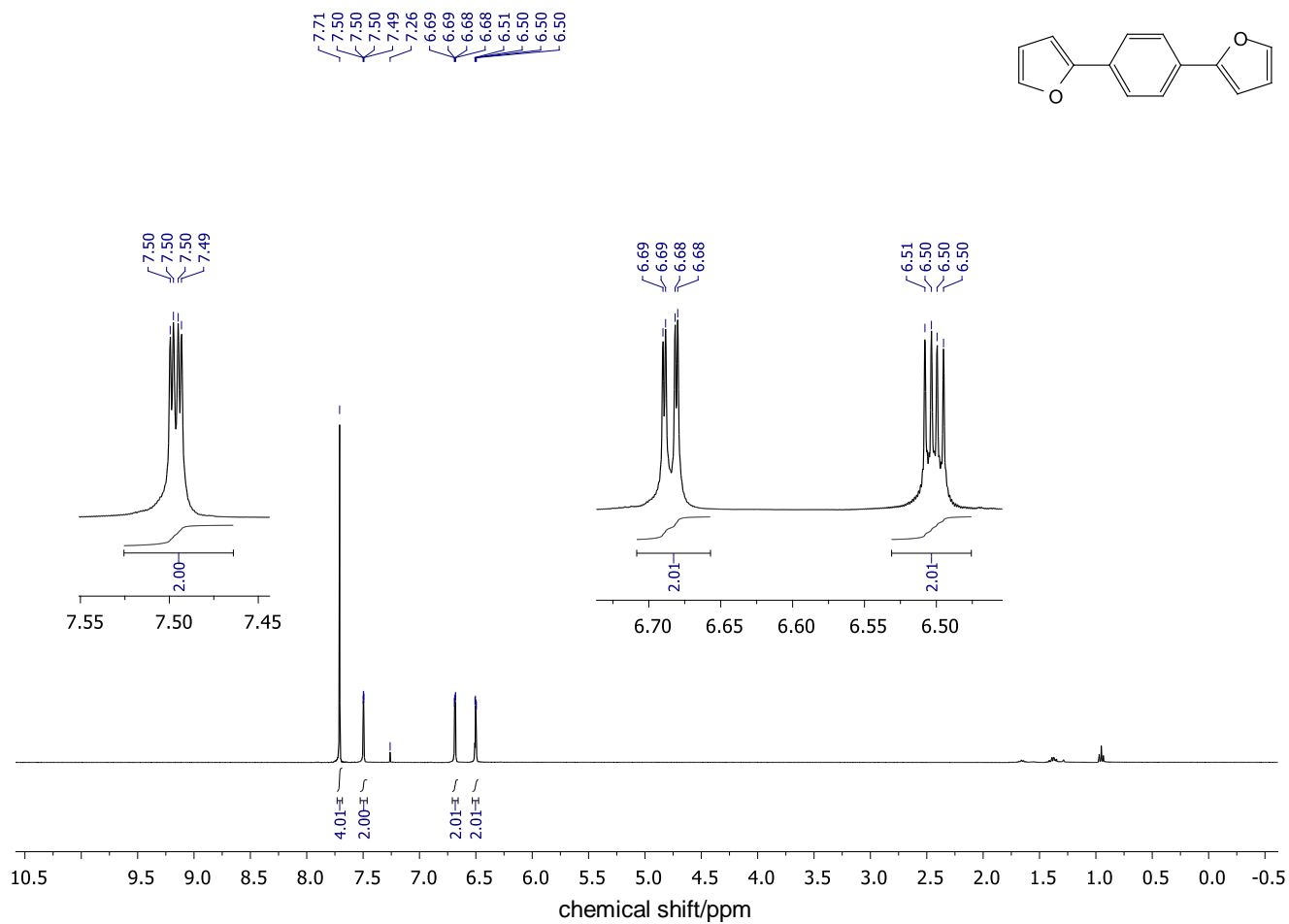


Figure S2. ¹H NMR spectrum of compound **2** in CDCl₃.

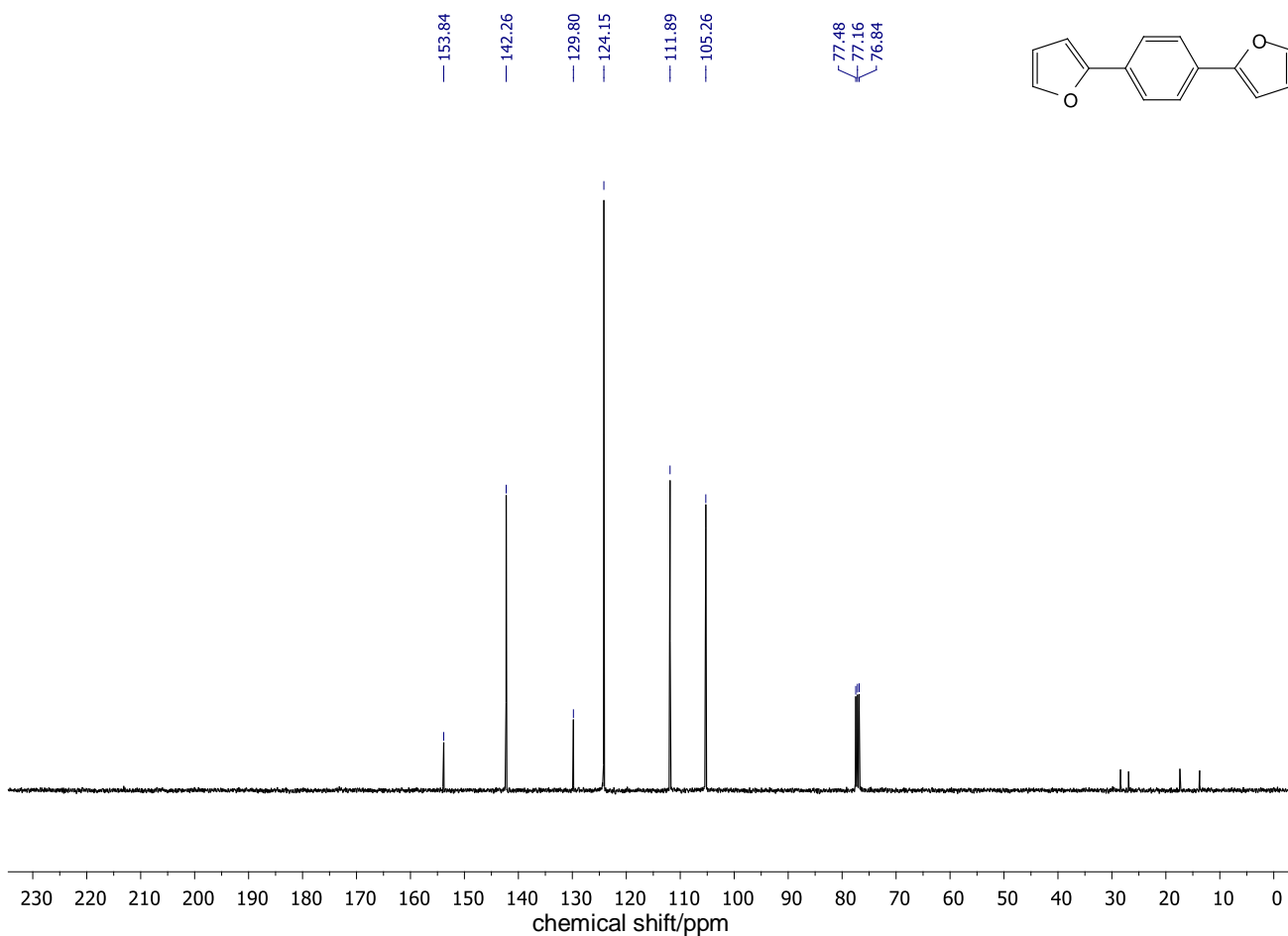


Figure S3. ^{13}C NMR spectrum of compound **2** in CDCl_3 .

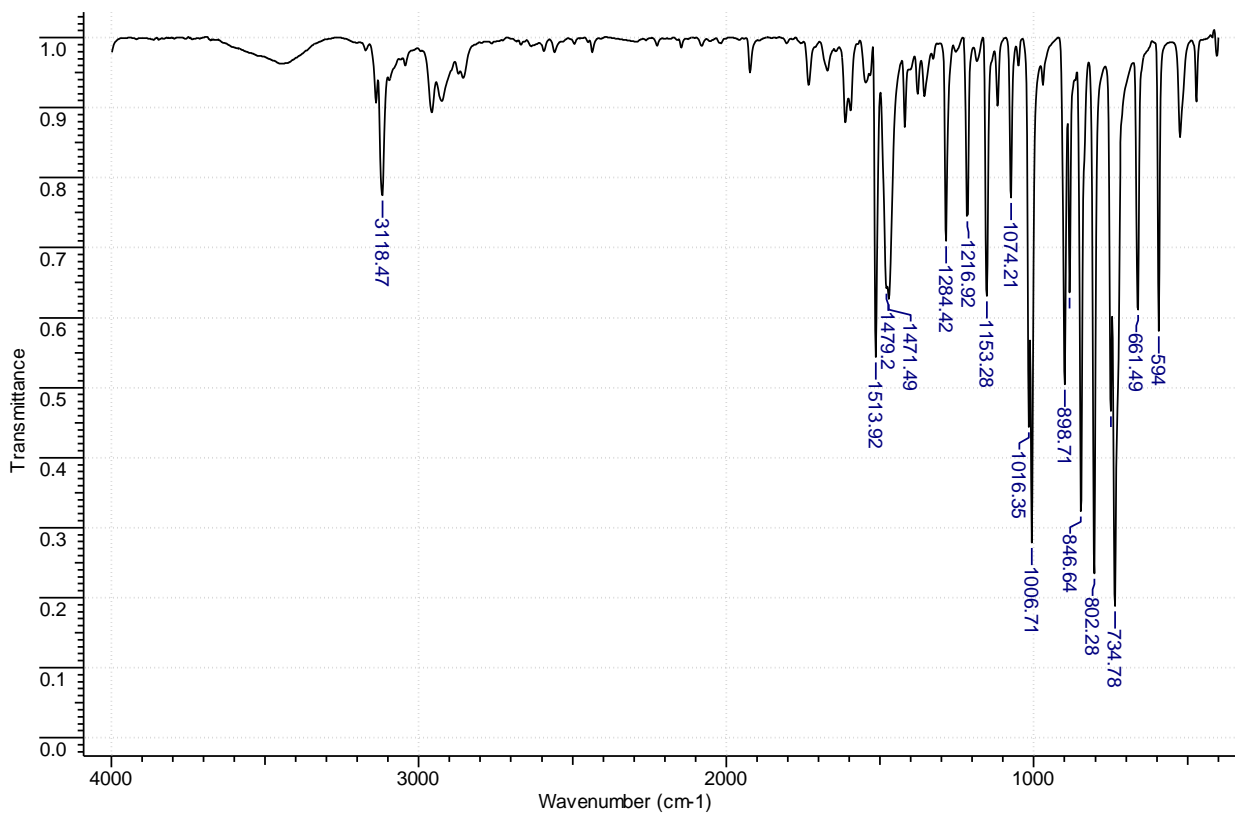


Figure S4. IR spectrum of compound **2** in KBr.

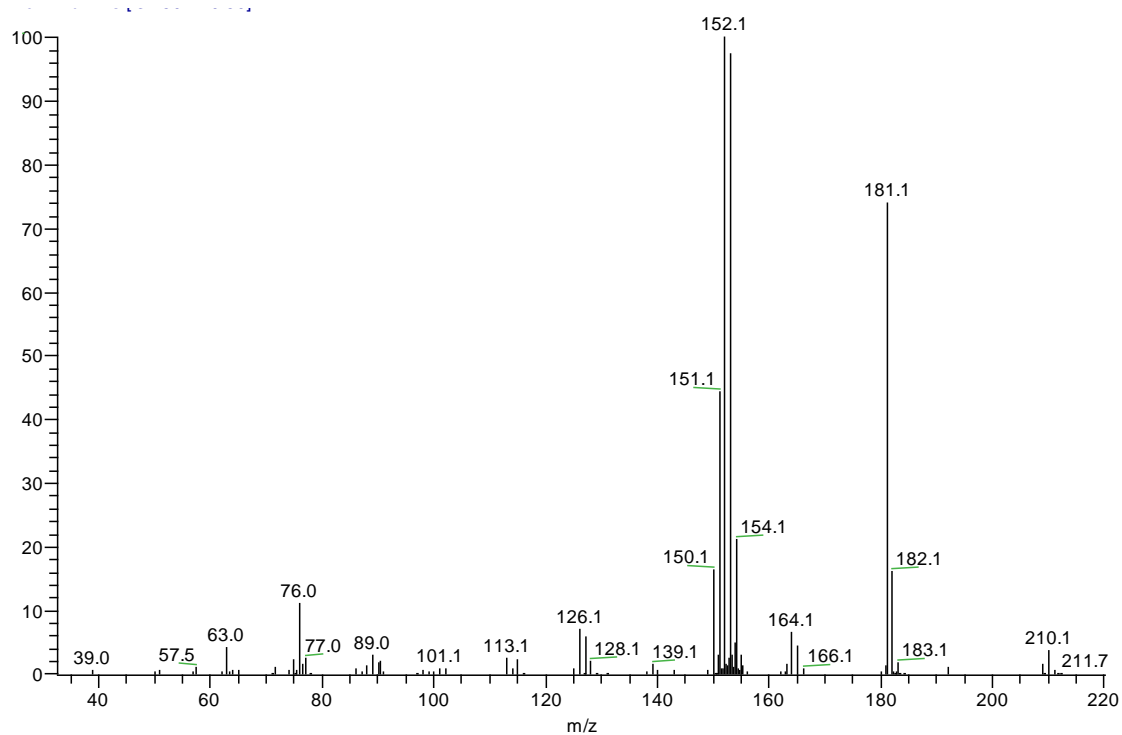


Figure S5. HRMS spectrum of compound **2**.

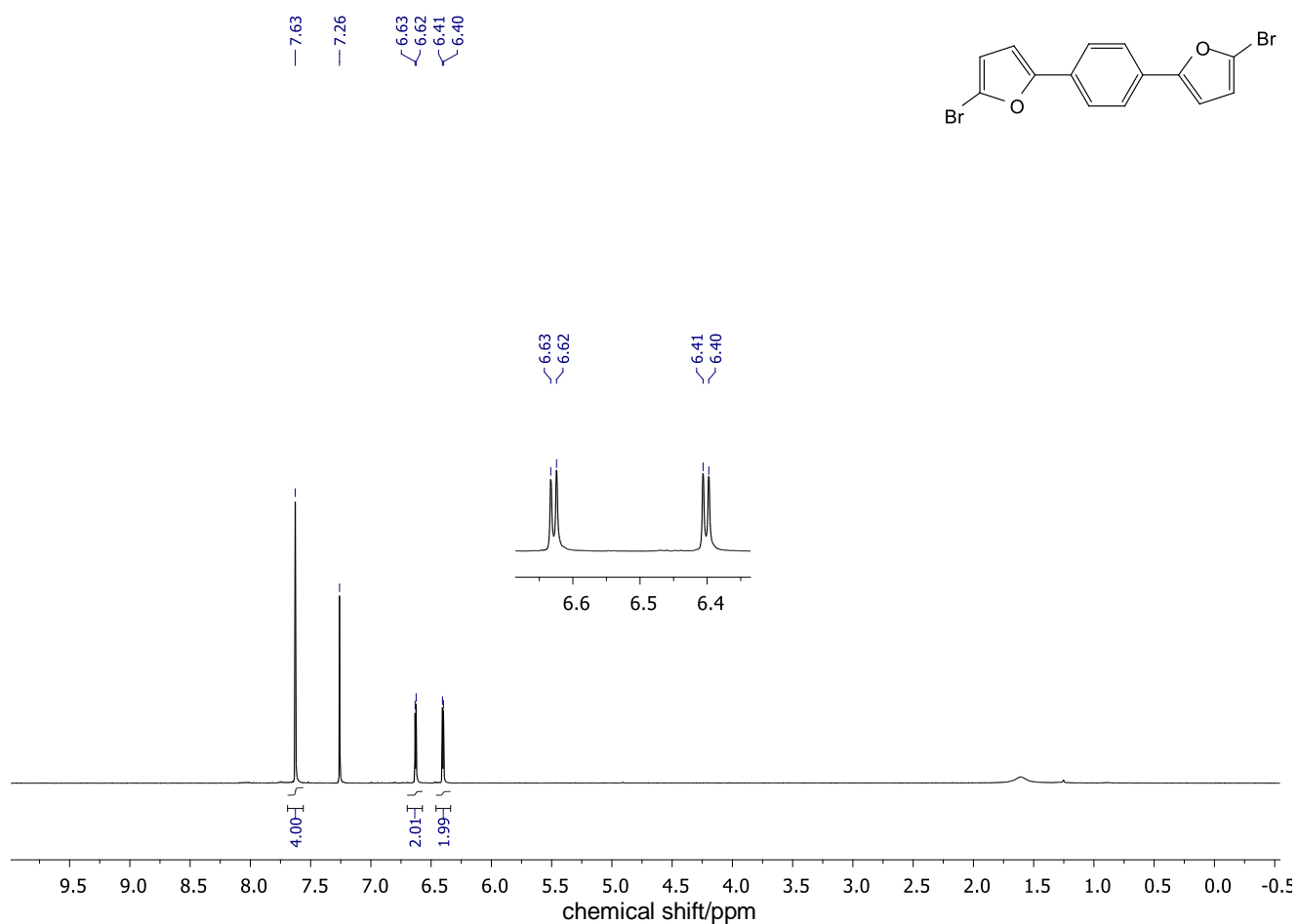


Figure S6. ^1H NMR spectrum of compound **3** in CDCl_3 .

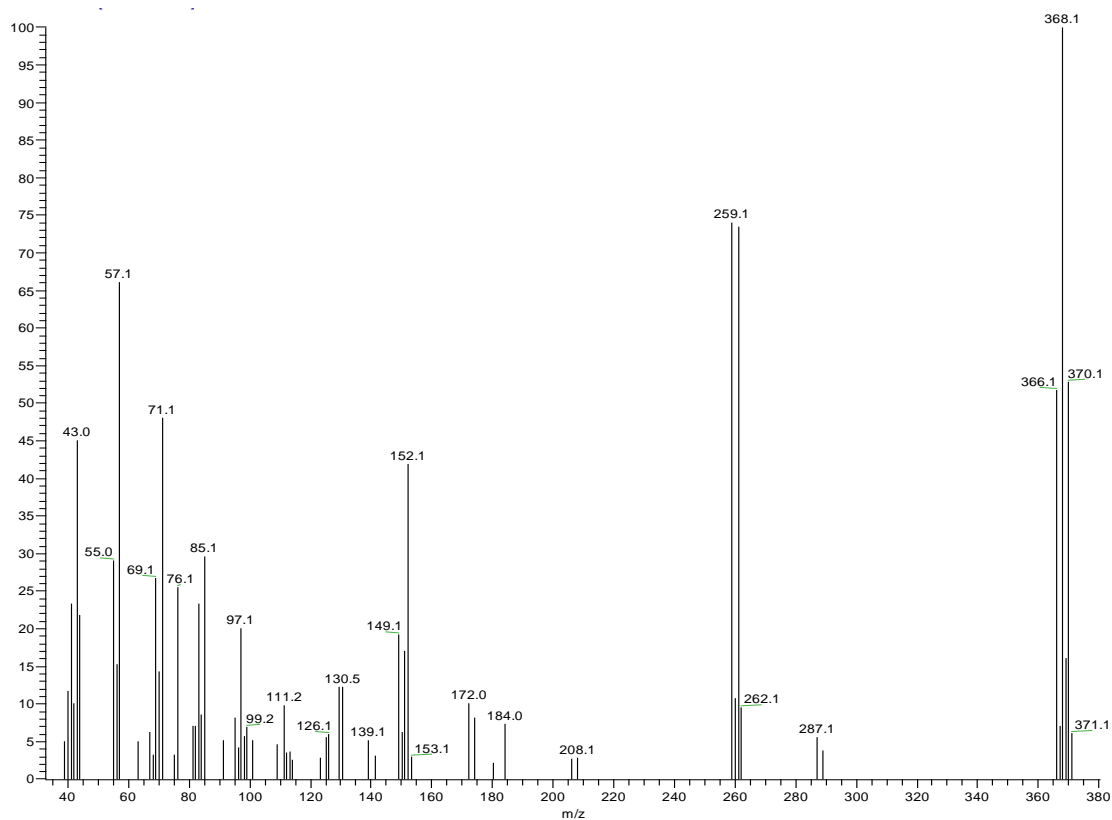


Figure S7. HRMS spectrum of compound **3**.

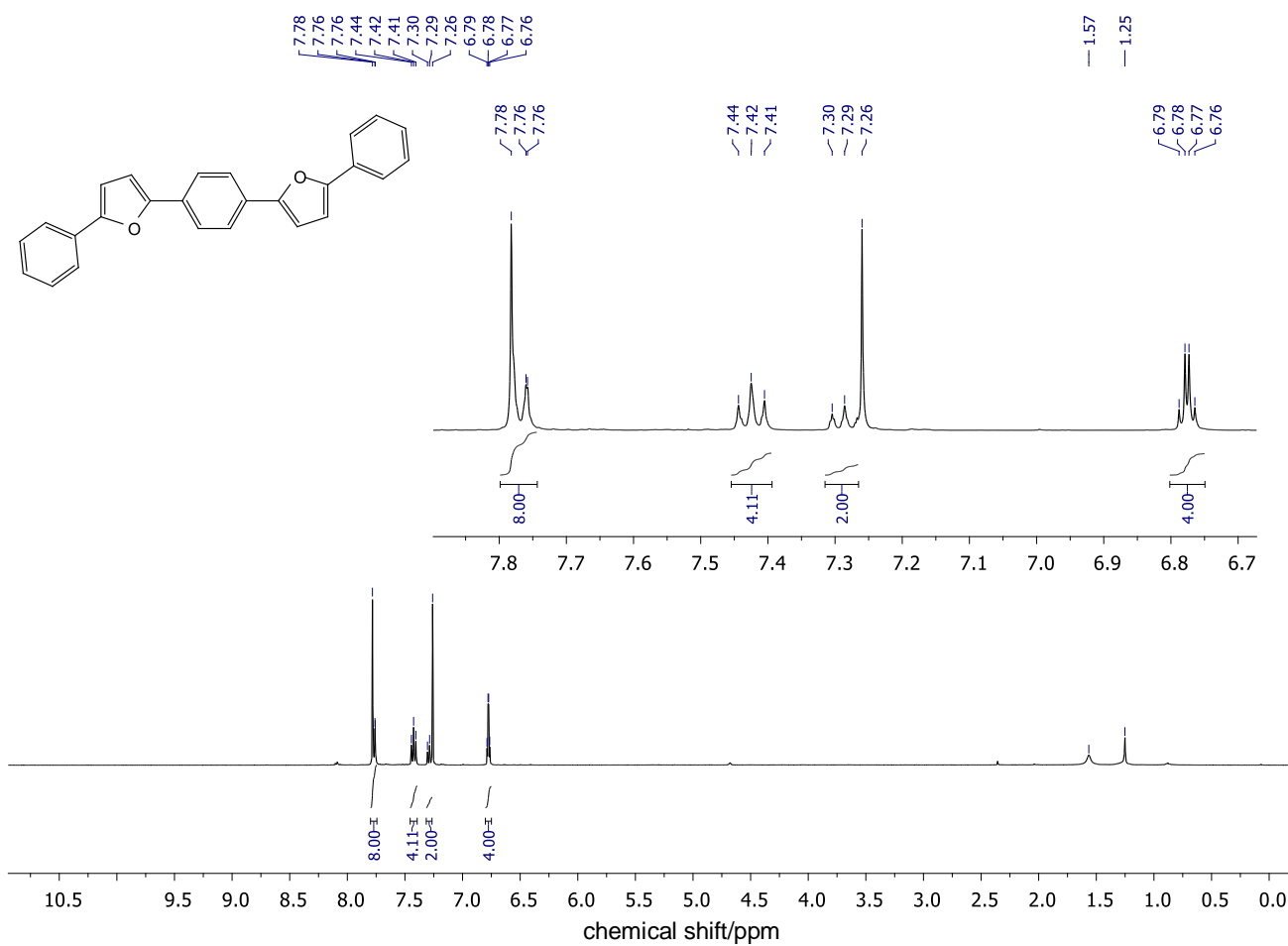


Figure S8. ¹H NMR spectrum of **4** in CHCl₃.

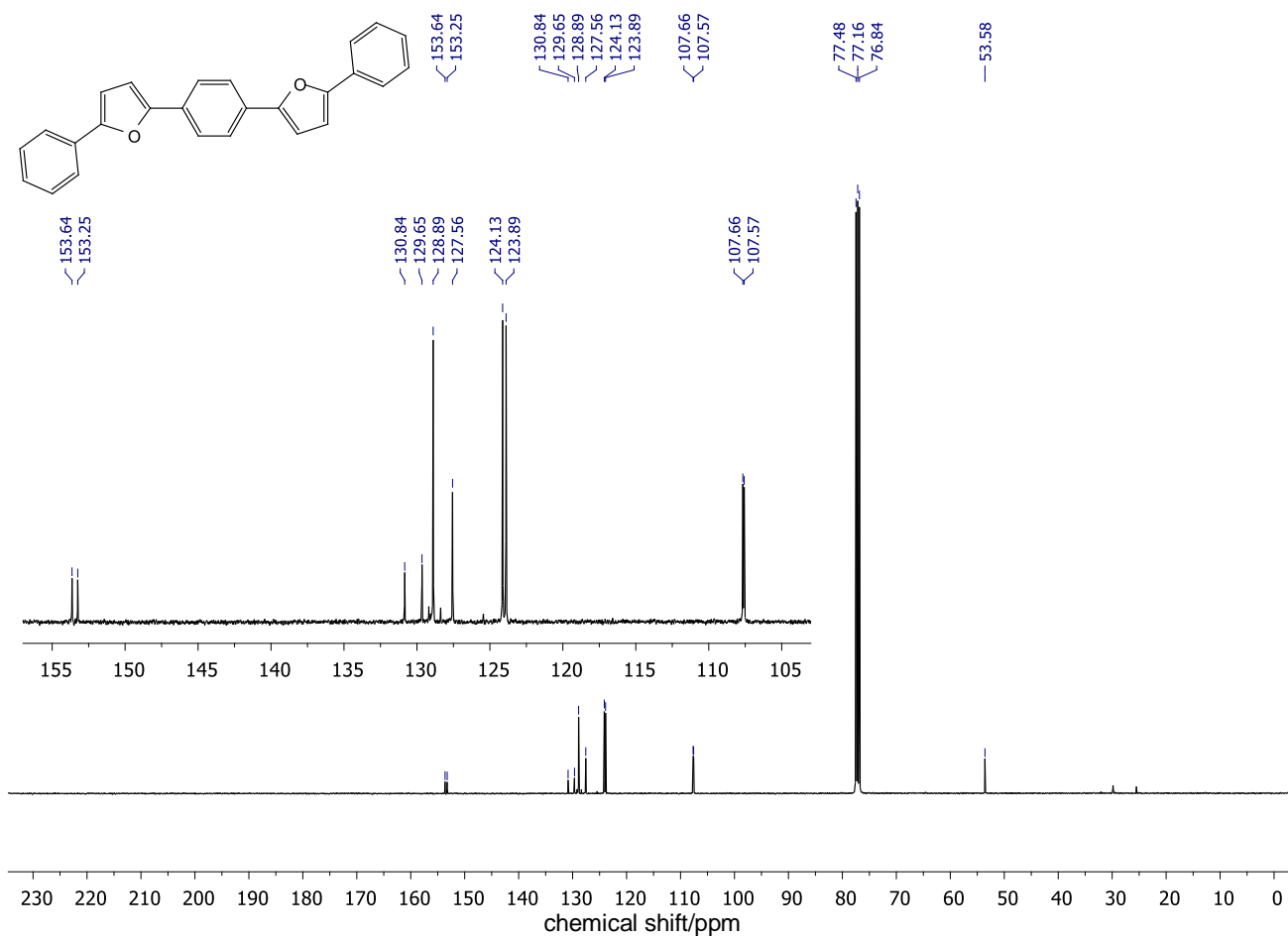


Figure S9. ¹³C NMR spectrum of **4** in CHCl₃. Peak at 53.6 ppm from CH₂Cl₂ impurities.

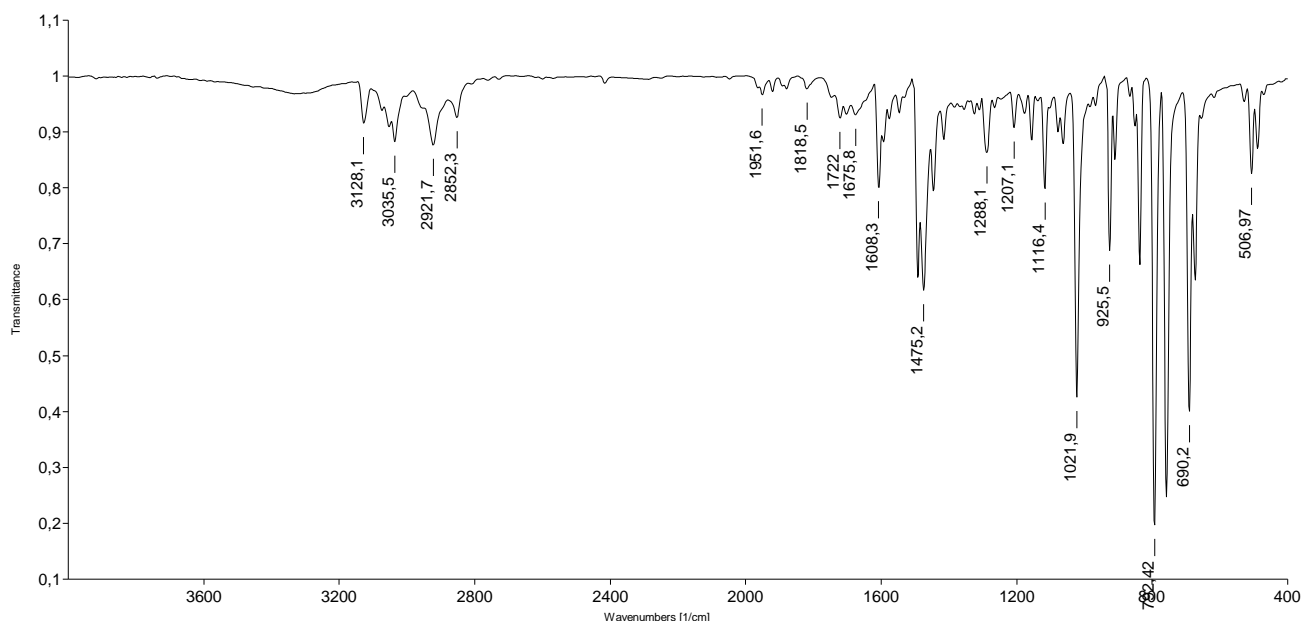


Figure S10. IR spectrum of **4** in KBr.

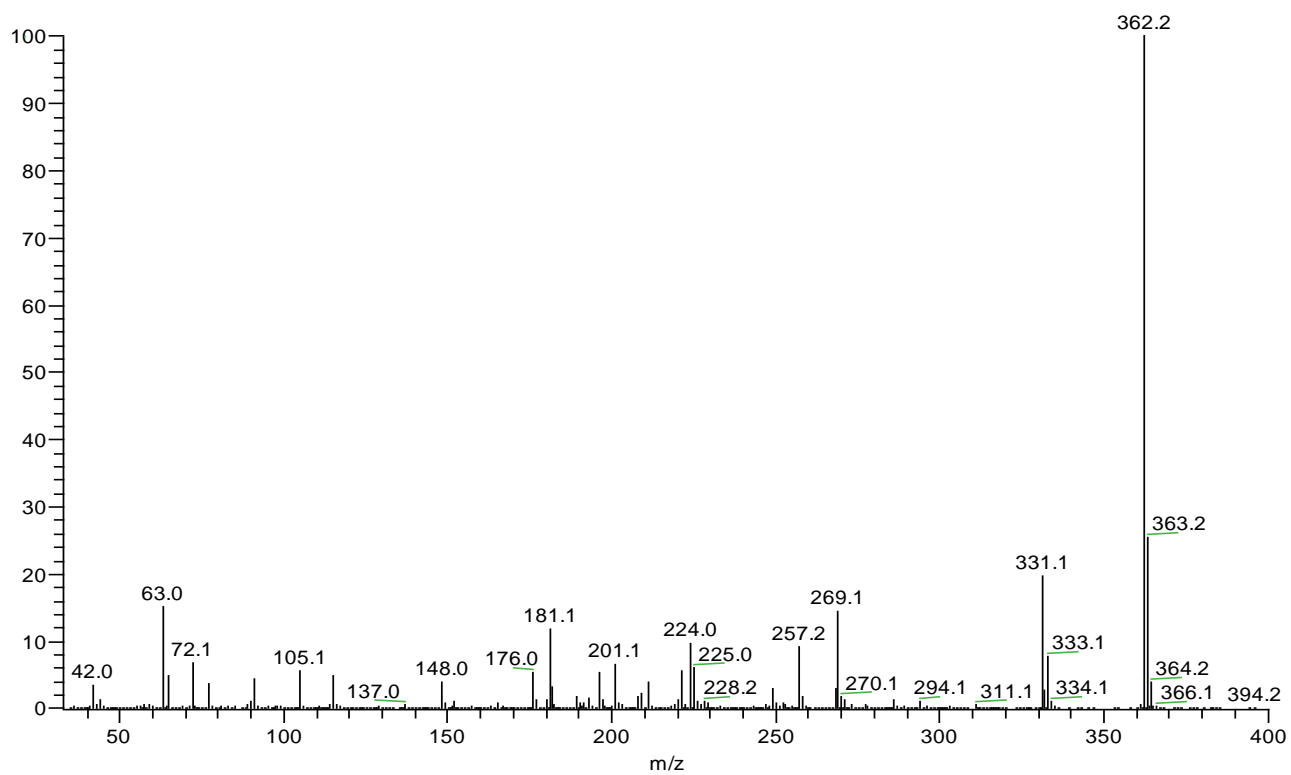


Figure S11. HRMS spectrum of **4**.

4. Thermal and CVA analysis

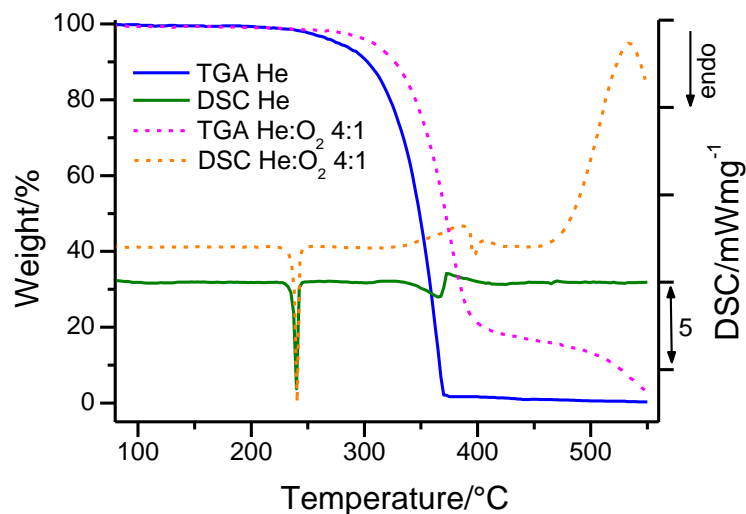


Figure S12. Thermogravimetric (TGA) and differential scanning calorimetry (DSC) analysis of BPFB in inert (helium, solid lines) and oxidizing (He:O₂=4:1, dashed lines) atmospheres.

Cyclic voltammetry measurements of BPFB were performed in CH₂Cl₂ solution. Within the electrochemical stability of the solvent, BPFB reduction was not observed. **Figure S13** shows the first reversible oxidation peak, the second peak is irreversible indicating decomposition. The HOMO energy level was estimated using the onset oxidation potential measured vs Fc/Fc⁺ as

$$E_{\text{homo}} = -e(E_{\text{onset}}^{\text{ox}} + 4.8) \text{ (eV)}.$$

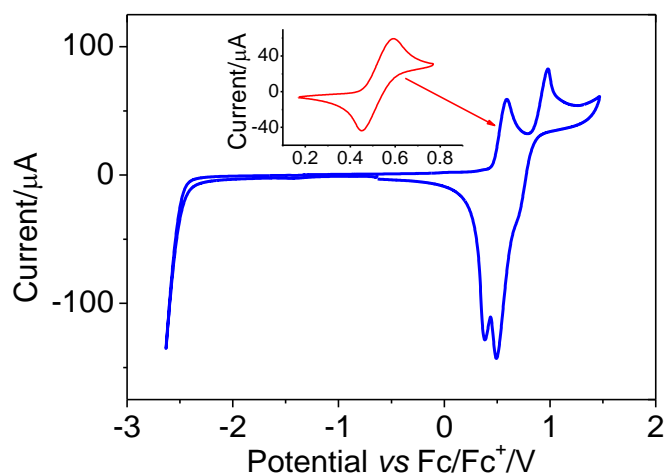


Figure S13. Cyclic voltammograms of BPFB in CH₂Cl₂. Inset is the first Ox/Red peak.

5. Microscopy

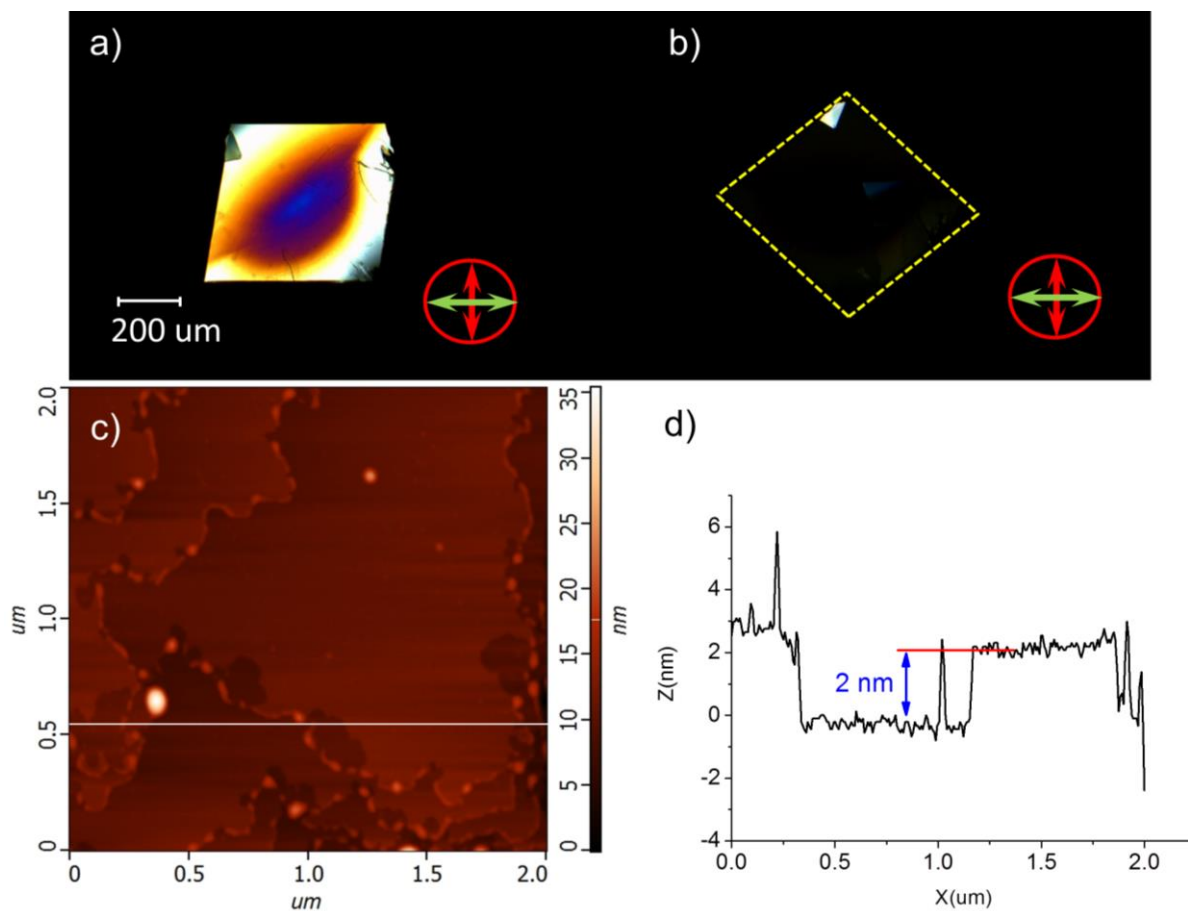


Figure S14. a) Optical image of a solution-grown BPFb single crystal in transmitted light through the crossed polarizers; b) the crystal is oriented in the dark state; the arrows indicate the orientation of polarizer (red) and analyzer (green); c) atomic force microscopy image and d) height profile of the surface of BPFb single crystal.

6. X-ray study

The details of the X-ray diffraction data are as follows: $V = 914.7(2) \text{ \AA}^3$, $Z = 2$, $D_{\text{calcd}} = 1.316 \text{ g} \cdot \text{cm}^{-3}$, $\mu(\text{Mo-K}\alpha) = 0.082 \text{ mm}^{-1}$, $F(000) = 380$, (θ 1.01–25.09°, completeness 99.9%), $T = 200(2) \text{ K}$, light-yellow rhombic plate, $(0.62 \times 0.60 \times 0.01) \text{ mm}^3$, transmission 0.780–0.862, 15386 measured reflections in index range $-24 \leq h \leq 24$, $-8 \leq k \leq 8$, $-7 \leq l \leq 7$, 1628 independent ($R_{\text{int}} = 0.0404$), 127 parameters, $R_1 = 0.0369$ (for 1264 observed $I > 2\sigma(I)$), $wR_2 = 0.1237$ (all data), GOOF 1.186, largest diff. peak and hole 0.165 and $-0.269 \text{ e} \cdot \text{A}^{-3}$.

The molecular structure and numbering of BPFB are shown in **Figure S15a**. The interplane angles between the furan rings and the central benzene unit are 13.1° (10.3 and 8.9° for thiophene-phenylene analog **AC5**) and between the furan rings and the terminal phenyls are 14.6° (9.9 and 7.8° for **AC5**).¹² The molecular length (the distance between *p*-hydrogens of terminal phenyls) is 19.03 \AA , and the atoms deviate from the average molecular plane within $\pm 0.55 \text{ \AA}$. The molecules have slightly zigzag-like form with the interplane angle between the central benzene and terminal phenyl rings 18.3° (16.2 and 12.7° for **AC5**). Therefore, BPFB is less planar than its thiophene-phenylene analogue **AC5** (**Figure S15b**).

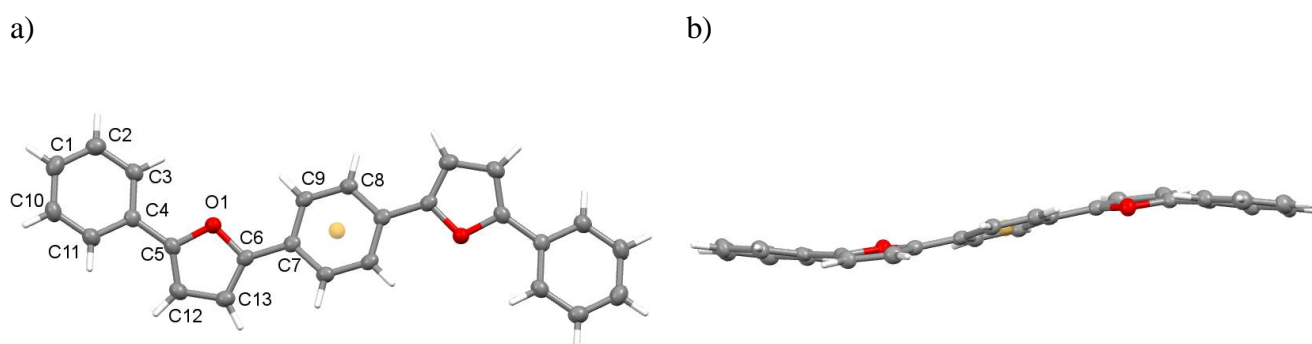


Figure S15. Molecular structure and numbering of BPFB with the symmetry center (yellow dot) at front (a) and side (b) views.

Table S1 Intermolecular C-H... π interactions in crystals of BPFB.

Interaction	H...Cg ^a , (\AA)	D _{pln} ^b , (\AA)	C-H...Cg ^a , ($^\circ$)
C2-H... π (C1C2C3C4C10C11)	2.76	2.74	137
C8-H... π (C7C9C8C7'C9'C8')	2.82	2.78	136
C11-H... π (C1C2C3C4C10C11)	2.84	2.82	137

^aCg- center of aromatic ring; ^bD_{pln}-distance H-atom to aromatic ring plane

7. Quantum chemistry calculations

Preliminary optimization was performed with AM1 from MOPAC 2012.¹³ The final geometry optimization was done with ORCA 3.0.1¹⁴ package by DFT B3LYP using a balanced polarized triple-zeta basis set def2-TZVP.^{15,16} Excited states were calculated by TD DFT B3LYP using the same basis set and the RIJCOSX approximation. All visualizations were done by using Gabedit 2.4.8¹⁷ or Avogadro¹⁸ software. Electronic properties of BPFB were calculated by optimizing geometry as well using X-ray data. Table S2 shows energy of frontier orbitals calculated by both methods. **Figure S16** demonstrates electron densities calculated from X-ray geometry (isovalue=0.03). The lowest singlet state was estimated to be 3.21 eV and triplet state 2.27 eV; $\Delta E_{ST}=0.94$ eV.

Table S2 Energy of frontier orbitals of BPFB.

	Optimized geometry	X-Ray geometry
E_{LUMO} , eV	-1.82	-1.70
E_{HOMO} , eV	-5.09	-5.10

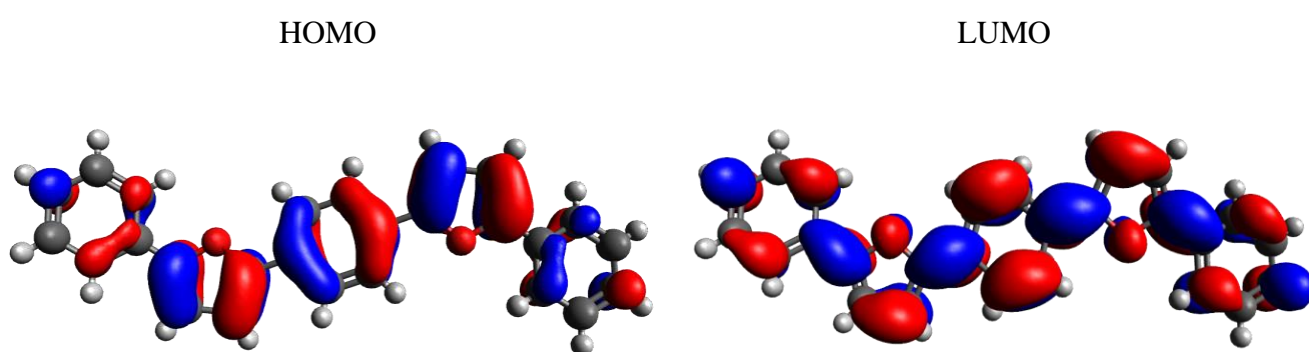


Figure S16. Calculated electron density on frontier orbitals of BPFB.

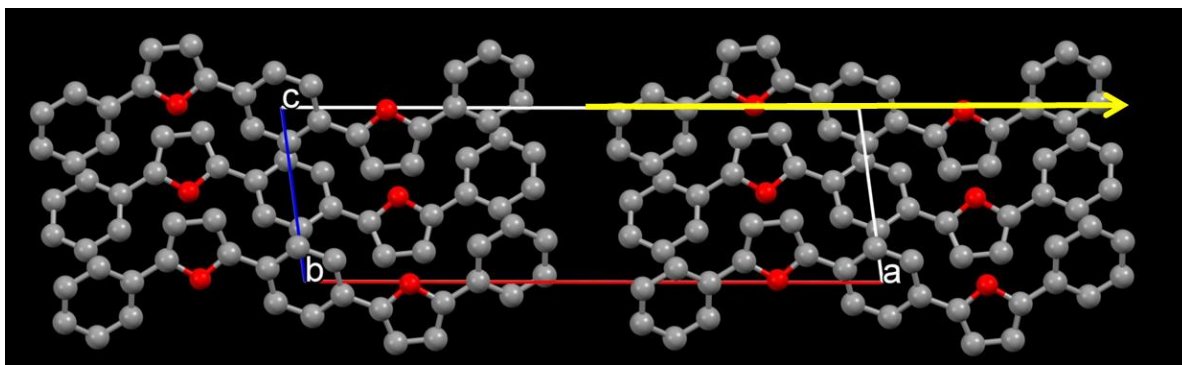


Figure S17. Transition dipole moment (yellow arrow) along the molecule calculated from the X-ray geometry.

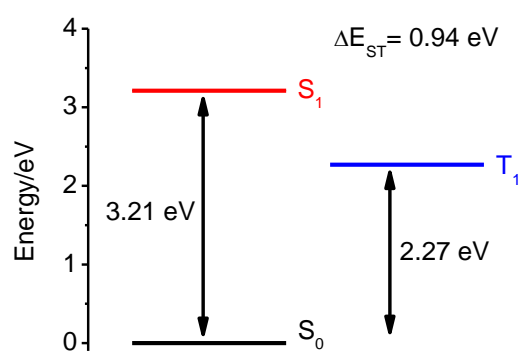


Figure S18. Excited states calculated by TD DFT.

8. OFET Data

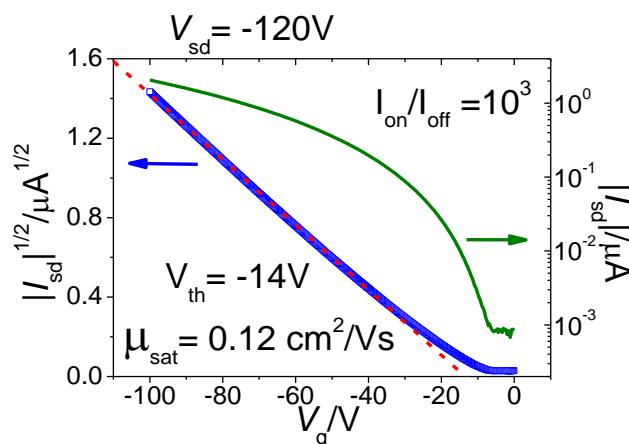


Figure S19. Transfer characteristics in the saturation regime of the device in **Figure 2** of the main text; V_{sd} , V_g and V_{th} are source-drain, gate and threshold voltages, respectively, μ_{sat} is the charge mobility extracted from the saturation regime.

Table S3. Parameters of fabricated single-crystal OFETs. W , L are channel width and length respectively; d and C are the thickness and capacitance of the dielectric layer, correspondingly.

Sample number	W [mm]	L [mm]	W/L	d [μm]	C [nF/cm ²]	μ_{lin} [cm ² /Vs]	μ_{sat} [cm ² /Vs]	V_{th} [V]
1	0.85	0.31	2.7	1.7	1.4	0.07	0.07	-17
2	1.15	0.41	2.8	1.6	1.5	0.12	0.12	-14
3	1.65	0.32	5.1	1.3	1.8	0.12	0.11	-14
4	0.44	0.37	1.2	1.5	1.6	0.06	0.07	-17
5	1.09	0.5	2.2	1.5	1.6	0.10	0.10	-13
Average						0.09±0.03	0.09±0.03	-15±2

9. Photoluminescence quantum yield

Figure S20 presents three experimental configurations needed for PL QY measurements, following de Mello and co-workers.¹⁹ In configuration **a**, the intensity of the scattered light of the excitation laser, L_a , is recorded. After this, a sample is placed in the sphere out of the laser beam (configuration **b**), and the intensity of the scattered laser light attenuated by the sample absorption, L_b , and the PL intensity due to sample excitation by the scattered laser light, P_b , are recorded. Finally, the sample is placed right in the laser beam (configuration **c**) to measure the intensity of the scattered laser light attenuated by the sample absorption in both the direct beam and the scattered light, L_c , and the PL intensity, P_c . All values L and P are integrals from the corresponding spectra calculated in terms of numbers of the laser and luminescence photons, respectively. All the spectra measured are presented in **Figure S21a**.

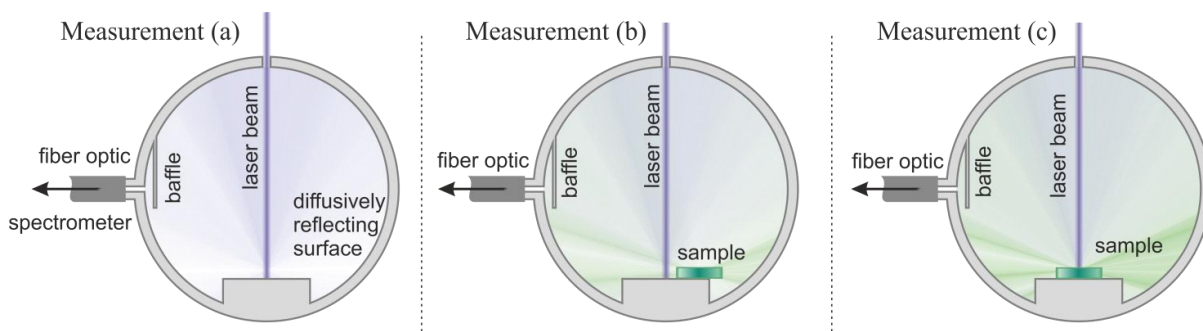


Figure S20. Three experimental configurations for PL QY measurement.

Finally, the fraction of directly absorbed laser photons A and the PL QY η are calculated as

$$A = 1 - \frac{L_c}{L_b};$$

$$\eta = \frac{P_c - (1 - A)P_b}{L_a A}.$$

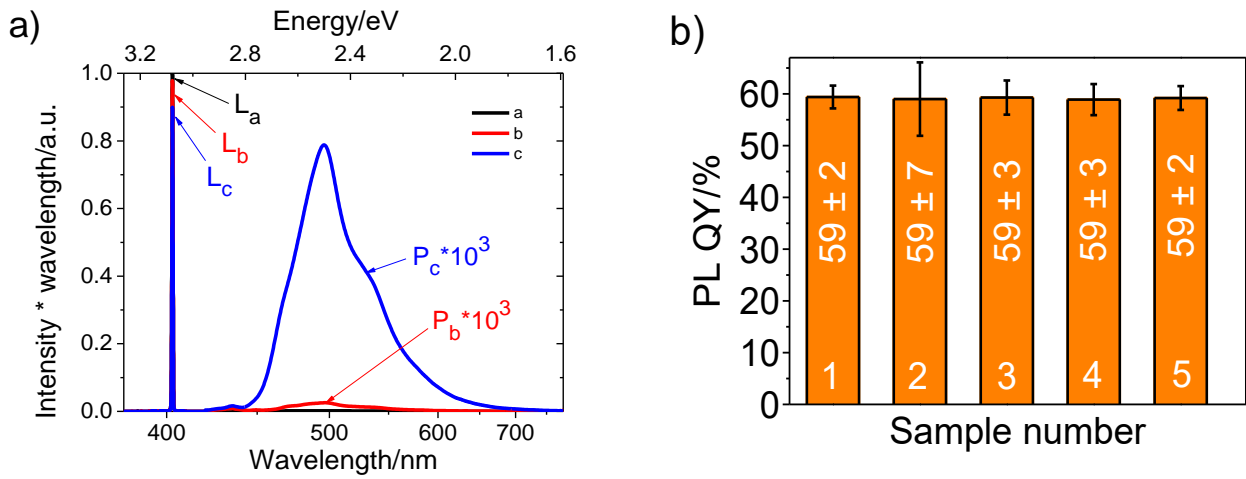


Figure S21. Typical spectra (a) and PL QY for series of 5 BPFB single crystals measured in the integrating sphere (b). The error bars include the calibration inaccuracy and the laser power fluctuations.

To evaluate the internal PL QY, η_0 , of the single crystals, we used the following expression²⁰

$$\eta_0 = \frac{\eta}{1 - p + p\eta},$$

where η is the (external) PL QY and p is the reabsorption probability. As the reabsorption effect is suggested to be negligible in the grinded crystal, we calculated p as a fraction of the reabsorbed photons

$$p = \frac{N_g - N_s}{N_g},$$

where N_s and N_g are integrals over the corresponding single and grinded crystals PL spectra in

Figure S22.

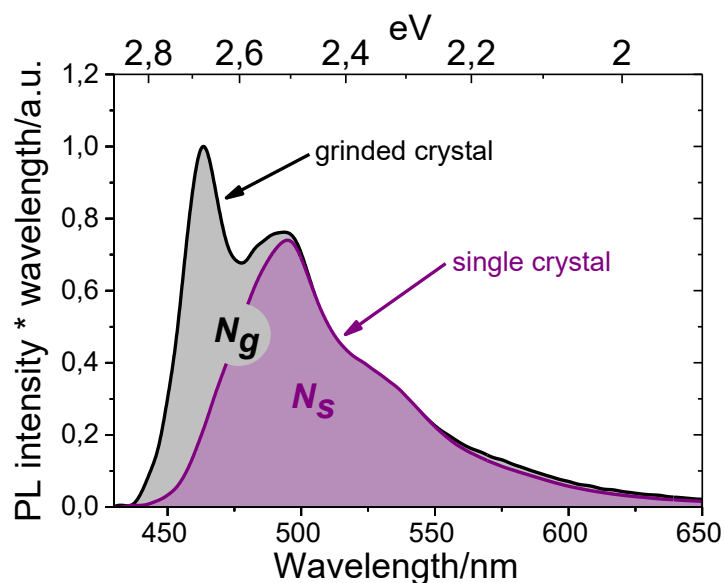


Figure S22. PL spectra of the single and grinded crystals from **Figure 3a** (main text) superimposed at the long-wavelength range where reabsorption is insignificant. The vertical axis shows a number of photons, i.e. the product of the PL intensity and the wavelength.

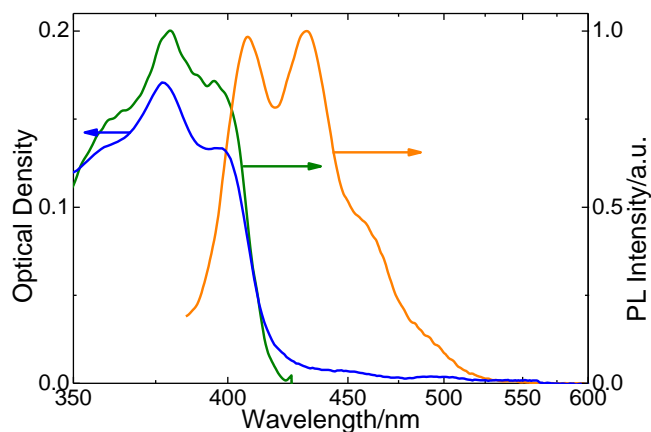


Figure S23. BPFb/PMMA solid-solution. (a) Excitation (olive, 435 nm detection wavelength) and PL (orange, 370 nm excitation wavelength) spectra of 85 mg/L BPFb/PMMA solid solution drop-casted on a glass substrate and absorption spectrum (blue) of a BPFb solid solution with concentration increased by a factor of 5 (425 mg/L). The excitation and PL spectra are normalized to their maxima.

10. Photoluminescence kinetics

Figure S24 summarizes PL spectra, time-resolved kinetics, and spectral diffusion data in different BPFb samples (single crystal, drop-cast, solutions) recorded using the streak-camera at 77 and 293 K. The monoexponential room-temperature PL decay time of 2.2 ± 0.1 ns in the single crystal does not change upon cooling to 77 K (**panel b**). Weak spectral diffusion (i.e. the temporal shift of the transient PL spectrum) in the single crystal (**panel c**) is temperature independent that can be ascribed to ordered molecular packing in the crystal.

The PL spectrum of the drop-cast sample is noticeably broader than that of the single crystal, presumably due to larger heterogeneities (**Figure S24d**). The PL decay in the drop-cast sample at room temperature becomes bi-exponential with two characteristic times of 0.3 ± 0.1 ns (75%) and 1.4 ± 0.1 ns (25%), and strongly temperature dependent (**Figure S24e**). Finally, the spectral diffusion at 293 K in the drop-cast sample (**Figure S24f**) is considerably stronger as compared to that in the single crystal (170 ± 5 meV vs. 40 ± 5 meV) and shows prominent temperature dependence. Thus, the PL of the drop-cast sample is consistent with thermally-activated exciton migration in the strongly disordered energy landscape²¹ due to high concentration of exciton traps or/and quenching sites. This is in sharp contrast with the single crystal where thermally activated hopping appears to be substantially reduced. Finally, the diluted liquid and solid solutions, where intermolecular interactions are switched off, show similar PL properties (**panel g, h, i**). The PL spectrum is substantially shifted to the blue as compared to the single-crystal and drop-cast samples as expected for non-interacting molecules in a weakly polarizable matrix. No spectral diffusion is observed in the solutions (**panel i**) as the molecular excitation resides at the same site.

Figures S25 compares PL spectra of BPFb samples in the 90° and 180° -geometries of PL collection. In the latter, the PL was collected in the microscopic arrangement mainly from the excitation spot of ~ 5 μm resulting in a minimal PL reabsorption effect. Here, the PL high-frequency onset at 435 nm is clearly observed, whereas in the 90° -geometry with the excitation spot of ~ 100 μm , the PL blue part is reabsorbed following in a very weak PL signal at 435 nm.

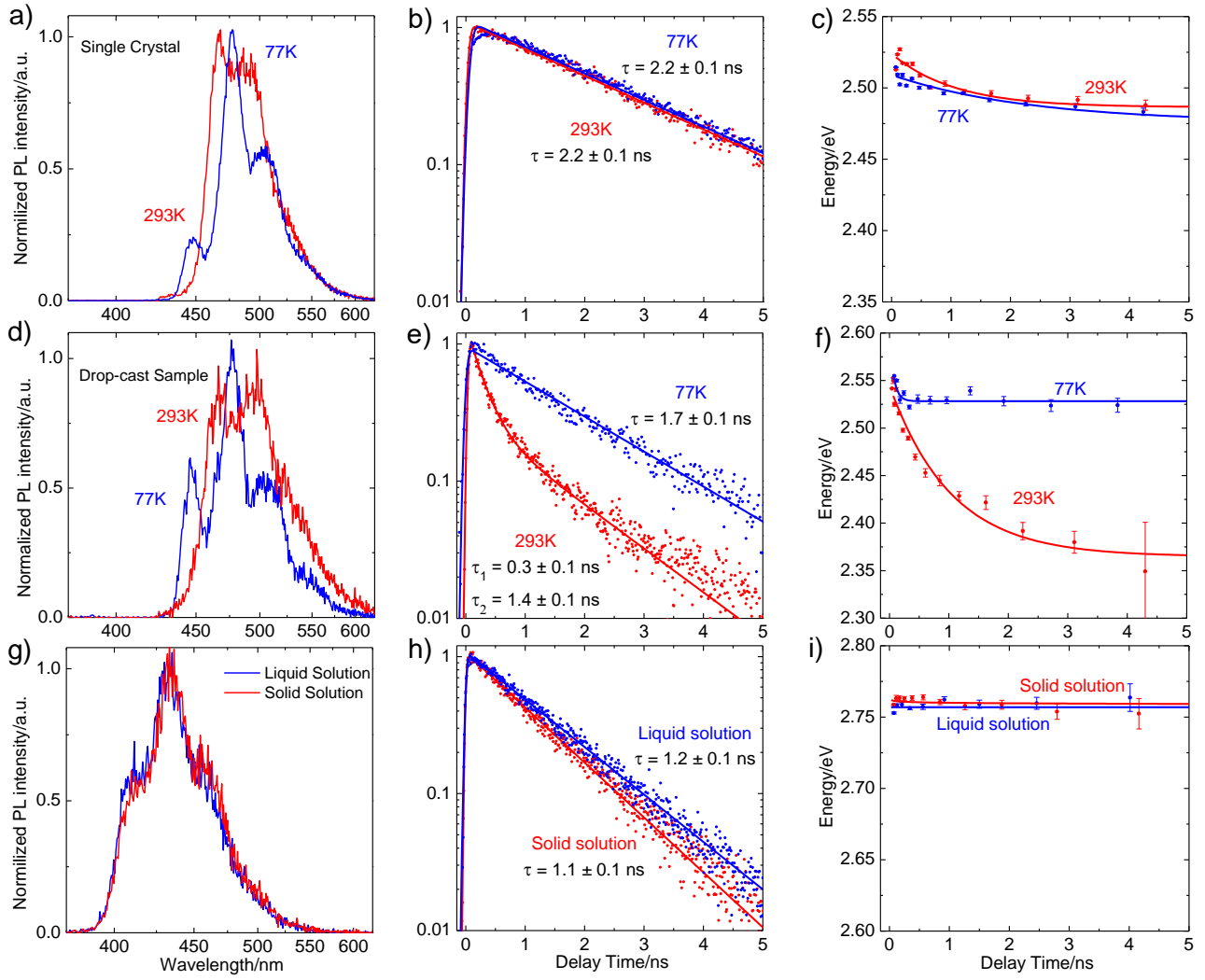


Figure S24. PL spectra (left), time-resolved kinetics (middle) and spectral diffusion (right) in BPFb single crystal (first row), drop-cast sample (second row), solutions (third row) recorded at 77 and 293 K. The PL excitation wavelength was 400 nm for the single-crystal/drop-cast sample (a-f) and 385 nm for the solutions (g-i). The kinetics were integrated over 425–550 nm (b, e) and 400–525 nm (h). The lines in (b, e, h) and (e) are mono- and bi-exponential fits, respectively convoluted with an apparatus response. The time-dependent mean energy values of the PL spectrum are shown in (c, f, i). The solid lines are exponential fits which amplitude ΔE provides an estimate for the energetic disorder as the following: in the crystal (c), $\Delta E_{77K} = 25 \pm 5$ meV, $\Delta E_{293K} = 40 \pm 5$ meV; in the drop-cast sample (f), $\Delta E_{77K} = 25 \pm 5$ meV, $\Delta E_{293K} = 170 \pm 5$ meV; in the solution (i), $\Delta E_{293K} = 0$ meV.

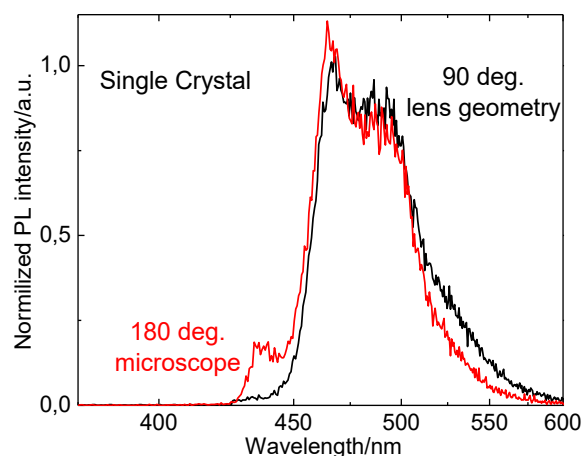


Figure S25. PL spectra of a BPFb single crystal at room temperature recorded by the streak camera at two different configurations of PL collection: 90°-geometry with a converging lens (focal length of 7.5 cm, excitation spot of ~100 μm) and 180°-geometry with a microscope objective (10x, NA=0.25) focusing the excitation beam into a spot size of ~5 μm. The excitation wavelength was 400 nm. The spectra are arbitrarily normalized. The 0-0 transition at 440 nm is suppressed in the 90°-geometry because of PL reabsorption.

11. References

1. H. Shang, H. Wang, N. Gao, F. Shen, X. Li and Y. Ma, *CrystEngComm*, 2012, **14**, 869-874.
2. V. A. Postnikov, Y. I. Odarchenko, A. V. Iovlev, V. V. Bruevich, A. Y. Pereverzev, L. G. Kudryashova, V. V. Sobornov, L. Vidal, D. Chernyshov, Y. N. Luponosov, O. V. Borshchev, N. M. Surin, S. A. Ponomarenko, D. A. Ivanov and D. Y. Paraschuk, *Cryst. Growth Des.*, 2014, **14**, 1726-1737.
3. SAINT, Data Reduction and Frame Integration Program for the CCD Area-Detector System, Bruker Analytical X-ray Systems, Madison, Wisconsin, USA 1997–2006.
4. G. M. Sheldrick, SADABS, Program for Area Detector Adsorption Correction, University of Goettingen, Goettingen, Germany, 1996.
5. G. M. Sheldrick, *Acta Crystallogr. Sect. A*, 2008, **A64**, 112-122.
6. V. Podzorov, V. M. Pudalov and M. E. Gershenson, *Appl. Phys. Lett.*, 2003, **82**, 1739-1741.
7. R. W. I. De Boer, M. E. Gershenson, A. F. Morpurgo and V. Podzorov, *Phys. Status Solidi*, 2004, **201**, 1302-1331.
8. A. M. Brouwer, *Pure Appl. Chem.*, 2011, **83**, 2213–2228.
9. A. Pelter, M. Rowlands and I. H. Jenkins, *Tetrahedron Letters*, 1987, **28**, 5213-5216.
10. P. A. Peart and J. D. Tovar, *Macromolecules*, 2009, **42**, 4449-4455.
11. K. Werbovetz, R. Brun, R. R. Tidwell, D. W. Boykin, M. A. Ismail, D. W. Wilson, R. K. Arafa, USA Patent EP1736466 (A1), 2006.
12. T. Yamao, Y. Taniguchi, K. Yamamoto, T. Miki, S. Ota, S. Hotta, M. Goto and R. Azumi, *Jpn. J. Appl. Phys.*, 2007, **46**, 7478-7482.
13. J. D. C. Maia, G. A. U. Carvalho, C. P. Manguiera Jr., S. R. Santana, L. A. F. Cabral and G. B. Rocha, *J.Chem.Theory Comput.*, 2012, **8**, 3072–3081.
14. F. Neese, *Wiley Interdiscip. Rev. Comput. Mol. Sci.*, 2012, **2**, 73-78.
15. F. Weigend and R. Ahlrichs, *Phys. Chem. Chem. Phys.*, 2005, **7**, 3297-3305.
16. A. Schaefer, H. Horn and R. Ahlrichs, *J. Chem. Phys.*, 1992, **97**, 2571-2577.
17. A.-R. Allouche, *J. Comput. Chem.*, 2011, **32**, 174–182.
18. M. D. Hanwell, D. E. Curtis, D. C. Lonie, T. Vandermeersch, E. Zurek and G. R. Hutchison, *J. Cheminform.*, 2012, **4**, 17.
19. J. C. deMello, H. F. Wittmann and R. H. Friend, *Adv. Mater.*, 1997, **9**, 230-232.
20. T.-S. Ahn, R. O. Al-Kaysi, A. M. Mueller, K. M. Wentz and C. J. Bardeen, *Rev. Sci. Instrum.*, 2007, **78**, 086105.
21. O. V. Mikhnenko, P. W. M. Blom and T.-Q. Nguyen, *Energy Environ. Sci.*, 2015, **8**, 1867-1888.